Materials Advances

ROYAL SOCIETY OF CHEMISTRY

PAPER

View Article Online
View Journal

Cite this: DOI: 10.1039/d5ma01077b

Enhanced gamma-ray shielding performance of Mn and Si-substituted AlPO-41 zeolite frameworks: a pathway to lightweight high-density protective materials

Z. Y. Khattari

The development of lightweight, efficient gamma-ray shielding materials is crucial for applications in nuclear energy, medicine and aerospace. This work introduces a novel materials design strategy by leveraging the atomic-scale tunability of microporous zeolite frameworks for radiation shielding, a significant departure from conventional composite-based approaches. We systematically investigate the shielding properties of the AlPO-41 zeolite framework and its derivatives—SAPO-41, MnAPO-41, and MnAPSO-41—through elemental substitution. Substituting Si and Mn into the framework increased its density from 3.855 g cm^{-3} (SAPO-41) to 3.897 g cm^{-3} (MnAPO-41) and significantly enhanced the effective atomic number (Z_{eff}), with MnAPO-41 reaching a maximum Z_{eff} value of 14.96 at 15 keV. The mass attenuation coefficient (MAC) was calculated over an energy range of 0.015–15 MeV. MnAPO-41 consistently demonstrated superior performance, with MAC values ranging from 9.064 cm^2 g^{-1} at 15 keV to 0.029 cm^2 g^{-1} at 5 MeV. A strong positive correlation between material density and linear attenuation coefficient was established, revealing a performance threshold for frameworks with densities >3.89 g cm^{-3}. These findings demonstrate that strategic Mn and Si substitution in zeolite frameworks is a highly effective strategy for designing high-performance, lightweight gamma-ray shielding materials.

Received 20th September 2025,
Accepted 14th November 2025

DOI: 10.1039/d5ma01077b

rsc.li/materials-advances

1. Introduction

Radiation shielding is a critical requirement in environments where ionizing radiation is present, such as nuclear power plants, medical radiology departments, and spacecraft.[1,2] Conventional materials like lead[3] and concrete[4] are commonly used for this purpose but their functioning is hampered by significant drawbacks, including excessive weight, lack of flexibility, and potential environmental toxicity.[5,6] To overcome these limitations, researchers have turned to advanced composite and nanostructured materials. This drive has spurred the development of a diverse range of alternatives, such as sustainable ceramic composites incorporating industrial waste like steel slag for enhanced attenuation,[7] advanced nanocomposites combining attapulgite clay with biochar and nickel oxide for superior shielding characteristics,[8] and doping of steel slag waste as a sustainable filler in ceramic tile composites for enhanced gamma-ray shielding, optimized through simulation for effective radiation blocking.[9] These studies highlight a common strategy: enhancing shielding by strategically incorporating specific elements or phases into a host matrix. Within this research landscape, advanced porous crystalline materials, such as aluminum phosphate-based frameworks (AlPOs), offer a uniquely promising alternative due to their structurally tunable properties at the atomic scale.[10]

Among this class of materials, the AFO-type zeolite frameworks—including AlPO-41,[10,11] SAPO-41,[12] and their metal-substituted variants like MnAPO-41 and MnAPSO-41[10]—are particularly noteworthy. These frameworks possess unique one-dimensional 10-ring channels with pore dimensions of 4.3–5.3 Å,[10] high framework densities (~19.1 T/1000 $Å^3$), and exceptional structural adaptability. This flexibility allows for the precise incorporation of specific elements, such as silicon (Si) or manganese (Mn), into their networks.[10–12] Elements like Si and Mn possess intermediate atomic numbers and exhibit moderate gamma-ray attenuation properties. Their introduction into the zeolite framework, either through direct substitution or pore-filling, can significantly enhance the shielding effectiveness of the resulting composites.[1,2]

The structural modifications resulting from silicon or metal substitution in these frameworks have been elucidated using advanced techniques like magic-angle spinning (MAS) NMR spectroscopy.[12] These alterations not only influence the framework's stability but also directly impact its radiation attenuation capabilities. For instance, Mn substitution in MnAPO-41

Department of Physics, Faculty of Science, The Hashemite University, P. O. Box 330127, Zarqa 13133, Jordan. E-mail: zkhattari@hu.edu.jo

enhances defect-site interactions, as evidenced by reversible changes in the NMR spectra during calcination and rehydration, while Si incorporation in SAPO-41 results in a less restricted framework structure.[12]

Despite these advancements, a significant gap remains in the development of shielding materials that are simultaneously lightweight, structurally well-defined, and tunable at the atomic scale. While composites and heavy-metal alloys improve upon lead and concrete, their properties are often averaged over a heterogeneous mixture, limiting precise control over the shielding mechanism. In contrast, crystalline microporous frameworks like zeolites offer a unique platform for systematic property engineering, yet their potential for radiation shielding remains largely unexplored and underexploited. This study addresses this gap by investigating the potential of the AFO-type zeolite (AlPO-41) and its iso-structural derivatives (SAPO-41, MnAPO-41, and MnAPSO-41) as a new class of lightweight, tunable gamma-ray shields. We hypothesize that strategic elemental substitution of Si and Mn into the framework will provide a powerful lever to control the density and effective atomic number (Z_{eff}), thereby directly enhancing attenuation properties. This work systematically assesses the relationship between atomic-scale composition, framework density, and gamma-ray attenuation across a broad energy spectrum. The findings aim to establish a foundational principle for the rational design of next-generation shielding materials based on compositionally tuned porous frameworks, moving beyond composite-based empiricism towards atomic-level design.[11–17]

2. Materials and methods

2.1 Density calculation

The theoretical bulk density (ρ) of each zeolite framework was calculated from its unit cell parameters. The density was derived from the unit-cell molar mass (M_w) and the unit-cell volume (V_c) using Avogadro's number ($N_A = 6.022 \times 10^{23}$ mol^{-1}), using the following equation:

$$\rho_z = \frac{M_w}{V_c N_A}$$

For each composition (AlPO-41, SAPO-41, MnAPO-41, and MnAPSO-41), M_w was determined by summing the atomic masses of all framework atoms within a single unit cell, including any substituted Si or Mn atoms. The unit-cell volume was obtained from high-resolution crystallographic data reported in the literature.[10–12] The resulting calculated densities are presented in Table 1 and demonstrate the incremental increase in mass density achieved through elemental substitution.

The data in Table 1 compare the densities of the pure AlPO-41 framework and its substituted variants. The observed increase in density for the frameworks incorporating higher atomic number elements (Si and Mn) is a direct result of the added mass from these substituents. For instance, the incorporation of manganese (atomic number $Z = 25$, density = 7.21 g cm^{-3}) into the MnAPO-41 framework yields the highest composite density of 3.897 g cm^{-3}. This trend confirms that elemental substitution is an effective strategy for enhancing the material's bulk density, a property critically linked to gamma-ray shielding performance.

The systematic increase in density from AlPO-41 (ρ = 3.862 g cm^{-3}) to MnAPO-41 (ρ = 3.897 g cm^{-3}) highlights the role of denser constituent atoms in improving attenuation capabilities. These calculated density values form the foundational basis for interpreting the shielding results discussed in subsequent sections (Fig. 1–5), where a consistent correlation between higher density and improved gamma-ray attenuation, particularly at lower photon energies, is observed.

2.2 Radiation shielding parameters

The mass attenuation coefficient (MAC), linear attenuation coefficient (LAC), and effective atomic number (Z_{eff}) were computed for each framework across a photon energy range of 0.015–15 MeV. The theoretical background and computational methodology, including details of the software packages used (*e.g.*, WinXCom), are described comprehensively in the SI.

3. Results and discussion

3.1 Gamma-ray shielding performance of substituted zeolite frameworks

3.1.1. Mass attenuation coefficients (MACs) across photon energy regimes. The gamma-ray shielding competence of the pure and substituted zeolite frameworks was evaluated by calculating their MACs over a broad energy range from 0.015 to 15 MeV. The overall trends are vividly captured in the 3D plot presented in Fig. 1, which illustrates the MACs for AlPO-41, SAPO-41, MnAPO-41, and MnAPSO-41 as a function of photon energy.

The data reveal three distinct attenuation regimes dominated by different photon–matter interactions. In the low-energy region ($0.015 < E < 0.2$ MeV), the photoelectric effect

Table 1 Comparison of densities for pure AlPO-41 zeolite[8,9] and its framework structures substituted heavy elements, highlighting their potential for radiation shielding applications along with the chemical formula, the mole and weight fraction of elements (in %) and density

AFO framework [reference]	AFO formula	Mole fraction of elements (%)					Weight fraction of elements (%)					Density (g cm^{-3})
		Al	P	O	Si	Mn	Al	P	O	Si	Mn	
AlPO-41[8,9]	$[Al_{20}P_{20}O_{80}]_{1/2}$	16.67	16.67	66.66	—	—	22.12	25.40	52.48	—	—	3.86181
SAPO-41[10]	$Si_{0.8}Al_{20.4}P_{18.8}O_{80}$	17.00	15.67	66.66	0.67	—	22.60	23.91	52.56	0.93	—	3.85562
MnAPO-41[10]	$Mn_{0.8}Al_{19.2}P_{20}O_{80}$	16.00	16.67	66.66	—	0.67	21.05	25.16	52.00	—	1.79	3.89722
MnAPSO-41[10]	$Mn_{0.8}Si_{0.8}Al_{19.2}P_{19.2}O_{80}$	16.00	16.00	66.66	0.67	0.67	21.07	24.18	52.05	0.91	1.79	3.89356

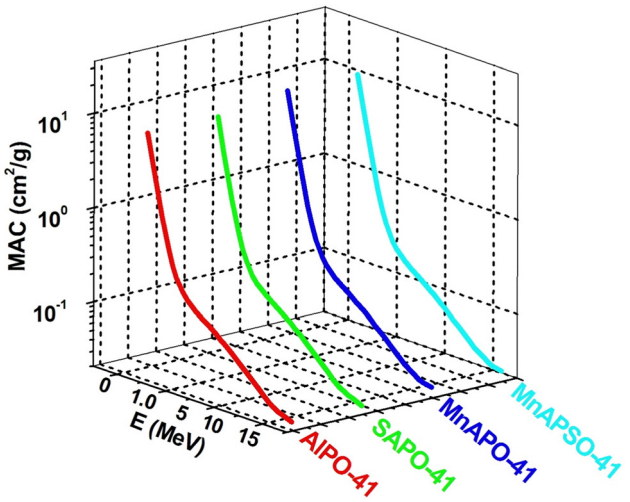

Fig. 1 A 3D illustration of the MAC values computed for the zeolite framework substituted with high-Z elements within the photon energy range of 0.015 < E < 15.0 MeV.

is the dominant process, resulting in high MAC values. As detailed in Fig. 2a, the MAC at 0.015 MeV is highest for frameworks incorporating manganese: MnAPO-41 (9.064 $cm^2\ g^{-1}$) and MnAPSO-41 (9.031 $cm^2\ g^{-1}$), compared to AlPO-41 (7.213 $cm^2\ g^{-1}$) and SAPO-41 (7.143 $cm^2\ g^{-1}$). This superior performance is a direct consequence of the higher Z_{eff} and density (see Table 2) imparted by Mn substitution, which significantly enhances photoelectric absorption. The MAC values for all materials decrease sharply with increasing energy, dropping to approximately 0.17 $cm^2\ g^{-1}$ around 0.1 MeV as the probability of photoelectric absorption diminishes.[14]

This behavior is consistent with fundamental radiation physics; at low energies, a photon's energy is comparable to the binding energy of inner-shell electrons, leading to a high probability of absorption. As photon energy increases, Compton scattering becomes increasingly significant, reducing the overall attenuation efficiency.[16] The observed trend aligns with studies on other systems; for instance, the MAC of α-quartz has been shown to be highly sensitive to structural parameters, emphasizing the general influence of material composition and density on shielding performance.[16]

In the intermediate-energy region (0.2 < E < 5.0 MeV, Fig. 2b), Compton scattering becomes the predominant interaction mechanism. Within this range, the MAC values for all frameworks drop significantly, from ~0.139 $cm^2\ g^{-1}$ to ~0.029 $cm^2\ g^{-1}$. The superior density of MnAPO-41 (3.897 $g\ cm^{-3}$, Table 1) continues to afford it a slight advantage, as Compton scattering probability is proportional to electron density.[14] Although pair production becomes energetically feasible above 1.022 MeV, its contribution to attenuation remains minimal until higher energies, resulting in a more gradual decline in MAC values compared to the low-energy region.[16–18]

Finally, in the high-energy region (E > 5.0 MeV), pair production becomes the dominant interaction. The MAC values for all samples plateau at a low level, ranging from 0.026 $cm^2\ g^{-1}$ at 5 MeV to 0.022 $cm^2\ g^{-1}$ at 15 MeV (Fig. 2b). This stability indicates a consistent, albeit reduced, capacity for attenuating high-energy gamma rays. The minimal variation between frameworks in this regime highlights that pair production is less sensitive to atomic number compared to the photoelectric effect. This consistency under high-energy conditions mirrors the behavior observed in other stable frameworks, such as berlinite ($AlPO_4$), which maintains consistent MAC values even under varying environmental conditions.[18]

Throughout all energy regimes, the data from Fig. 1 and 2 consistently demonstrate that MnAPO-41 exhibits the highest MAC values, followed by MnAPSO-41, AlPO-41, and SAPO-41. This hierarchy directly correlates with the trend in material density (MnAPO-41 > MnAPSO-41 > AlPO-41 > SAPO-41, Table 1), unequivocally establishing the critical role of density

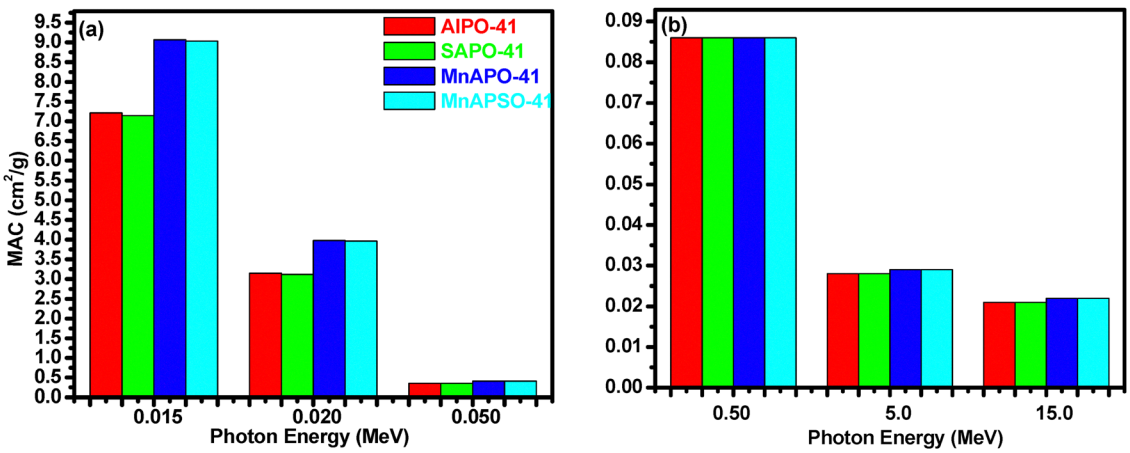

Fig. 2 A bar illustration of the MAC values computed for the pure and heavy-element-substituted zeolite framework structures at low (a) and high (b) photon energies. The MAC values of the Mn-based framework surpass those of other frameworks at low photon energy (E = 0.015 MeV), while MnAPO-41 exhibits marginally higher values at high photon energies. At energies greater than 0.40 MeV, the average MAC values are nearly equal, reflecting that high-Z element-substituted zeolite framework structures effectively attenuate gamma-rays due to their higher atomic numbers.

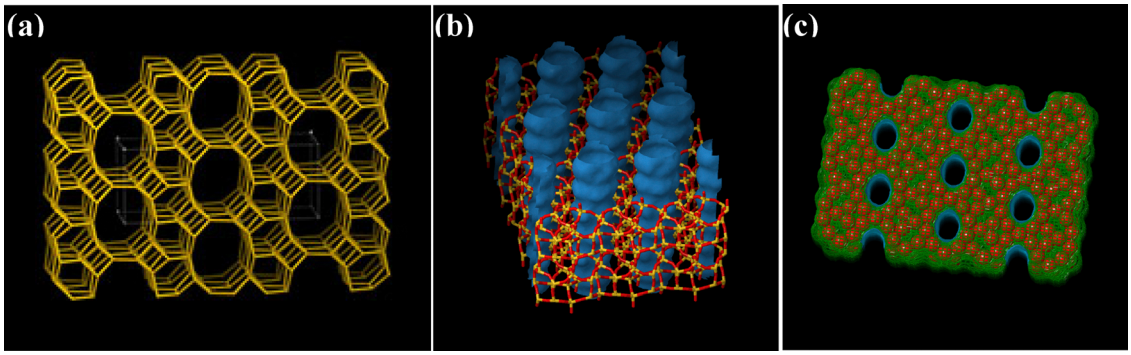

Fig. 3 Illustrations of the AFO framework presented as a cage model (a), a channel system using stick representation with a thickness of 0.25 (b), and a two-sided channel system in ball-and-stick representation (c). The AFO framework adopts a *Cmcm* (#63) point group and an orthorhombic structure. Its topological pore diameter is approximately 5.43 Å with >6-ring openings in a 1D channel system, demonstrating the effect of substituting Si, Mn, or both in the framework. The accessible pore volume of 7.23% highlights its potential for radiation shielding applications.

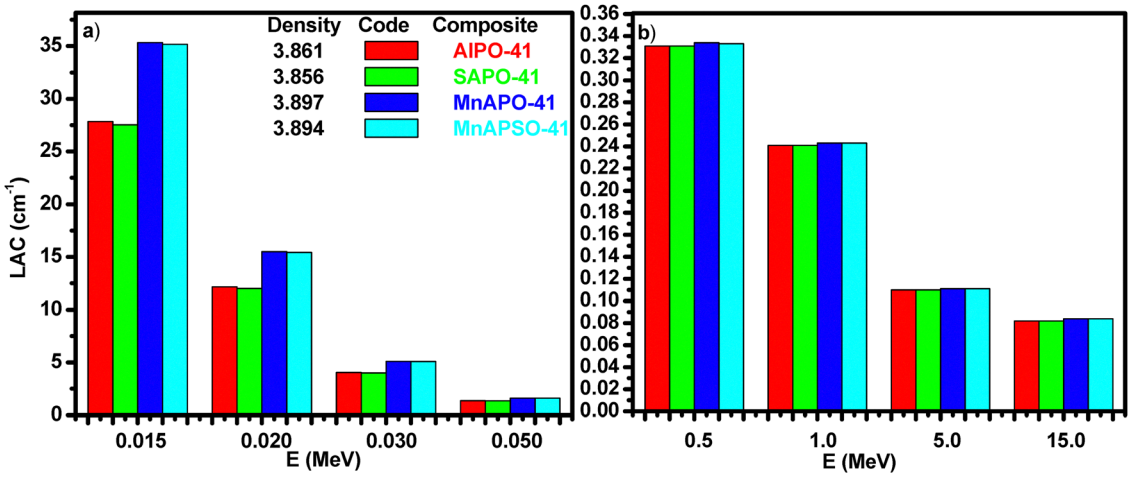

Fig. 4 Linear attenuation coefficients (LACs) of the studied high-*Z* element-substituted zeolite framework structures at selected low-photon energies (a) and high-photon energies (b). The figure also includes the density (in g cm^{-3}) and composite formulas of the structures. Results indicate that the MnAPO-41 composite outperforms all others in attenuating gamma-ray radiation, showcasing its superior shielding properties due to its high density and atomic number.

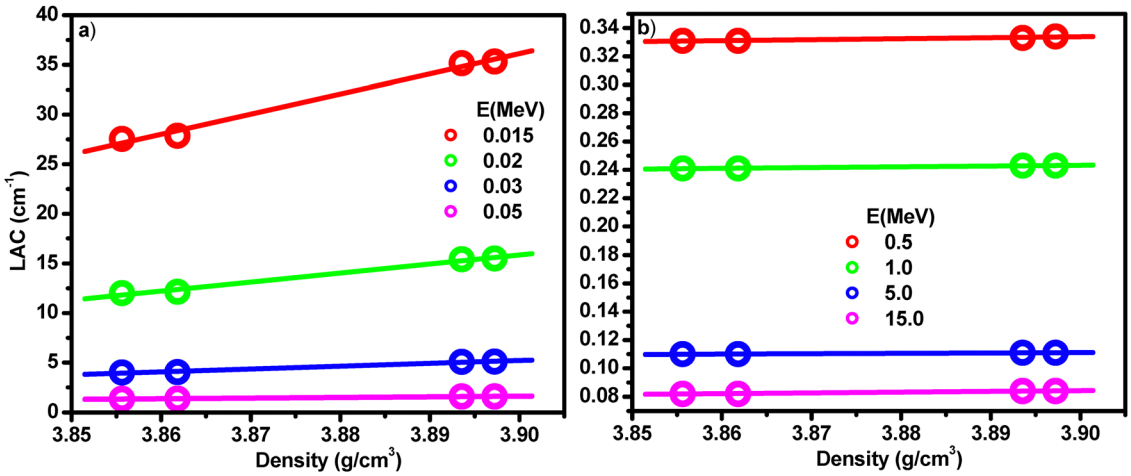

Fig. 5 Linear attenuation coefficients (LACs) of the studied high-*Z* element-substituted zeolite framework structures as a function of density at selected photon energies, as indicated in the figure. The data highlight the relationship between material density and gamma-ray attenuation, showcasing the superior performance of higher-density frameworks, particularly those substituted with elements like Mn or Si.

and elemental composition in enhancing gamma-ray shielding performance.[18,19]

3.1.2. Comparative analysis and the role of effective atomic number (Z_{eff}). The data from Fig. 1 and 2 clearly demonstrate that MnAPO-41 consistently exhibits the highest MACs across the entire photon energy spectrum, followed by MnAPSO-41, AlPO-41, and SAPO-41. This performance hierarchy is not arbitrary but is directly governed by the fundamental role of atomic number in gamma-ray interaction probabilities. The incorporation of higher atomic number elements like manganese ($Z = 25$) enhances these probabilities across all interaction mechanisms: photoelectric absorption, Compton scattering, and pair production.[1]

The most compelling evidence for this atomic number dependence is found in the calculated Z_{eff}, values presented in Table 2. At a low photon energy of 0.015 MeV, where the photoelectric effect dominates, the Z_{eff} values for the substituted frameworks (MnAPO-41 = 14.96 and MnAPSO-41 = 14.95) significantly exceed those of the pure frameworks (AlPO-41 = 13.28 and SAPO-41 = 13.23). This pronounced difference quantitatively confirms that Mn substitution successfully elevates the composite atomic number of the material, leading to the markedly higher MAC values observed in this energy regime (*e.g.*, MAC = 9.06 $cm^2\ g^{-1}$ for MnAPO-41 *vs.* 7.21 $cm^2\ g^{-1}$ for AlPO-41 at 0.015 MeV).

As the photon energy increases to 0.15 MeV, a noticeable decline in Z_{eff} for all frameworks is observed, signaling the diminishing contribution of the highly Z-dependent photoelectric effect and the increasing dominance of Compton scattering. In the intermediate energy range (1.5–5.0 MeV), the gap in Z_{eff} values between the substituted and pure frameworks narrows significantly, as Compton scattering has a weaker dependence on the atomic number. Despite this convergence, the Mn- and Si-substituted frameworks maintain a distinct, albeit smaller, advantage in their Z_{eff} and MAC values, highlighting their superior performance in practical shielding scenarios where radiation fields are often poly-energetic.[19–21]

At high energies ($E > 5.0$ MeV), where pair production becomes the dominant interaction, the Z_{eff} values for all materials gradually decrease and converge to approximately 11.3. This trend is consistent with the physical principles of pair production, whose cross-section has a quadratic dependence on atomic number (Z^2), but whose preponderance over other effects leads to a stabilization of the effective Z. This convergence explains the plateauing and narrowing of the MAC values at high energies, as seen in Fig. 2b.[20]

The critical need to incorporate higher-Z elements is further highlighted by the performance of SAPO-41. Despite containing silicon, its MAC and Z_{eff} values are the lowest of all four frameworks across most energies (Table 2), attributable to its lower overall density (3.856 g cm^{-3}, Table 1). This result underscores that both elemental composition and density must be optimized synergistically to achieve superior shielding performance, a principle also demonstrated in other material systems such as carbonate-based ceramics.[21]

This study aligns with a broader scientific effort to tailor material properties for radiation shielding. While previous work has explored silicon-based crystals[19,20] and complex cyclosilicates like $BaTi(SiO_3)_3$,[22] our findings specifically demonstrate the efficacy of using iso-structural substitution within microporous zeolite frameworks—a strategy that allows for precise tuning of Z_{eff} and density without altering the underlying mechanical and structural integrity of the material.[22]

3.1.3. Structural basis for shielding performance. The exceptional shielding performance of the substituted AFO-type zeolites is fundamentally rooted in their unique structural architecture, which provides an ideal platform for property tuning. As illustrated in Fig. 3, the AFO framework adopts an orthorhombic structure (space group *Cmcm*, #63) characterized by a stable, uniform arrangement of atoms. This structural integrity is crucial for maintaining framework stability during the substitution process.[18–22]

The framework's defining feature is its one-dimensional channel system, comprised of 10-ring openings with a topological pore diameter of approximately 5.43 Å (Fig. 3a). This specific geometry is not merely a structural curiosity; it creates accessible sites and pathways ideal for the incorporation of substituting elements like Si and Mn (Fig. 3b). The cage model (Fig. 3a) highlights the interconnected nature of this network, while the ball-and-stick representation (Fig. 3c) provides atomic-scale insight into the potential sites where substitution can occur, directly influencing local electron density—a key factor in gamma-ray interaction probabilities.[23–25]

Despite its capability to host additional mass, the framework remains light weight, with an accessible pore volume of 7.23%. This presents a significant advantage for designing shields that balance mechanical integrity with high attenuation performance.[25] The type of elemental substitution strategically tailors the shielding properties: silicon substitution primarily enhances the framework's structural rigidity and overall density, which directly improves attenuation performance, particularly in the

Table 2 The MAC ($cm^2\ g^{-1}$), LAC (cm^{-1}), and effective atomic number (Z_{eff}) values for the studied zeolite framework structures at selected photon energies (MeV), highlighting their gamma-ray interaction efficiency

	E = 0.015			E = 0.15			E = 1.5			E = 5.0			E = 10.0			E = 15.0		
AFO-type	MAC	LAC	Z_{eff}	MAC	LAC	Z_{eff}	MAC	LAC	Z_{eff}	MAC	LAC	Z_{eff}	MAC	LAC	Z_{eff}	MAC	LAC	Z_{eff}
AlPO-41	7.21	27.86	13.28	0.139	0.537	10.99	0.051	0.196	10.89	0.028	0.110	11.00	0.023	0.088	11.15	0.021	0.082	11.26
SAPO-41	7.14	27.54	13.23	0.139	0.536	10.97	0.051	0.196	10.86	0.028	0.110	10.97	0.023	0.088	11.13	0.021	0.082	11.23
MnAPO-41	9.06	35.33	14.96	0.141	0.550	11.33	0.051	0.198	11.12	0.028	0.111	11.27	0.023	0.090	11.48	0.022	0.084	11.62
MnAPSO-41	9.03	35.16	14.95	0.141	0.549	11.32	0.051	0.198	11.11	0.028	0.111	11.26	0.023	0.090	11.46	0.022	0.84	11.61

intermediate and high-energy regimes where Compton scattering and pair production dominate, while manganese substitution introduces a higher atomic number (Z = 25) into the structure. This dramatically enhances photoelectric absorption at low energies, as confirmed by the superior MAC and Z_{eff} values of MnAPO-41.[26]

The combination of both elements in MnAPSO-41 leverages a synergistic effect: Si stabilizes and densifies the framework, while Mn provides the high-Z component for effective photon capture. This makes the AFO framework a highly adaptable and promising candidate for the rational design of multifunctional radiation shielding materials. Further experimental and computational studies could focus on optimizing these substitutions to target specific energy ranges of interest. This has been observed in cyclosilicates.[22] It is also present in silicon carbide (SiC) crystals.[23]

3.1.4. Linear attenuation coefficients and the density–shielding relationship. The LAC provides a direct measure of a material's ability to attenuate radiation per unit thickness, making it a critical parameter for practical shielding applications. The LAC data, presented in Fig. 4, offer an unequivocal demonstration of the superiority of Mn-substituted frameworks.

Consistent with the MAC trends, MnAPO-41 exhibits the highest LAC values across the entire photon energy spectrum (Fig. 4a and b). This is a direct consequence of it possessing the highest density (3.897 g cm^{-3}, Table 1) among the studied frameworks, as the LAC is the product of the MAC and density (LAC = μ = MAC × ρ). At low energies (Fig. 4a), its performance is dominated by the high photoelectric cross-section of manganese (Z = 25). Even at higher energies, where Compton scattering prevails, its superior density ensures a higher probability of interaction, allowing it to maintain the lead in attenuation performance. MnAPSO-41 follows closely, benefiting from the synergistic combination of Mn's high atomic number and the structural density enhancement provided by Si.[24,25]

In contrast, AlPO-41 and SAPO-41 exhibit significantly lower LAC values, a direct reflection of their lower densities and the absence of high-Z elements like Mn. The minimal performance gap between MnAPO-41 and MnAPSO-41 is highly informative; it suggests that Si substitution can be used to fine-tune the framework's structural and mechanical properties without a drastic compromise in shielding efficiency, offering valuable flexibility for materials design.[24–26]

The paramount importance of density is masterfully illustrated in Fig. 5, which plots LAC directly against density for selected energies. This analysis reveals a strong, positive correlation between these two parameters. Frameworks with densities above approximately 3.89 g cm^{-3} (*i.e.*, those incorporating Mn or Si + Mn) consistently cluster in the high-performance region of the plot, unequivocally establishing density as the primary driver of shielding efficacy in these zeolitic systems. The trend is most pronounced at lower energies (*e.g.*, 0.5 MeV), where the photoelectric effect amplifies the benefit of high-Z, dense materials. At higher energies (*e.g.*, 15 MeV), the relationship, while still positive, plateaus, reflecting the decreasing dependence of Compton scattering on atomic number.[25,26] Other important shielding parameters can be found in Table S in the SI.

This work aligns with a growing body of research emphasizing the critical link between density, composition, and shielding. Similar positive correlations between density and LAC have been observed in systems ranging from carbonate-based ceramics to silicates.[26,27] Furthermore, studies have shown that external factors like pressure, which primarily act to increase density by modifying interatomic distances, can significantly enhance shielding performance,[24] reinforcing the fundamental principle demonstrated here: increasing density is a universally effective strategy for improving radiation attenuation.[27,28]

3.2 Materials design and optimization

The results of this study provide a clear path for designing and optimizing zeolite-based materials for gamma-ray shielding. The primary objective is to achieve an optimal balance between three key parameters: atomic composition, density, and structural integrity.

The most critical factor identified is density optimization. A strong, positive correlation exists between framework density and shielding performance, as unequivocally demonstrated by the LAC data in Fig. 5. Therefore, the primary design strategy should be to maximize density through strategic elemental substitution without compromising the stability of the zeolite framework.

Our findings indicate that frameworks with densities exceeding 3.89 g cm^{-3}—specifically those incorporating manganese (Mn) and silicon (Si)—deliver the best overall attenuation performance. The choice of the substituent element should be guided by the target photon energy spectrum:

- For superior low-energy shielding (<200 keV): Prioritize manganese substitution. Its high atomic number (Z = 25) maximizes the photoelectric effect, resulting in the highest MAC and Z_{eff} values, as seen in MnAPO-41.
- For tunability and structural reinforcement: Silicon substitution is highly advantageous. While it provides a more modest boost in density and Z_{eff} compared to Mn, it enhances the framework's mechanical rigidity and offers a pathway to fine-tune material properties. This makes compositions like MnAPSO-41 excellent candidates where a balance of shielding strength and material versatility is required.

Consequently, optimization strategies should focus on maximizing the incorporation of Mn to achieve the highest possible density and low-energy performance. For applications requiring a specific balance of properties, controlled co-substitution with Si presents a powerful method to tailor the framework.[22–25]

Furthermore, the energy-dependent behavior of the shielding parameters necessitates an application-specific design approach. Materials intended for shielding low-energy radiation (*e.g.*, in medical diagnostics) should be optimized for high-Z elements to leverage photoelectric absorption. In contrast, shields for mixed-field or high-energy environments (*e.g.*, around nuclear reactors) must prioritize high overall density to maximize efficiency in the Compton scattering regime.[26–28]

3.3 Validation and practical considerations

While this study establishes a strong theoretical foundation for the shielding performance of substituted AFO zeolites, we acknowledge the importance of experimental validation for practical assessment. To bolster confidence in our computational predictions, we compared our results with experimental and simulation data from recent, advanced shielding composites, including those highlighted by the reviewer.

A direct comparison reveals the promising potential of our designed frameworks. For instance, the MnAPO-41 framework in this work demonstrates a MAC value of 0.1157 $cm^2\ g^{-1}$ at E = 0.238 MeV. This performance is highly competitive when benchmarked against state-of-the-art composites.[9] It is notably a comparable MAC value of 0.1811 $cm^2\ g^{-1}$ at E = 0.238 MeV reported for the steel–slag composite at 40% filling in ref. 9.

Furthermore, the performance hierarchy and design principles established in our study align with the fundamental strategies confirmed in other advanced shielding systems. For example, ref. 8 demonstrated that increasing the concentration of high-Z nickel oxide (NiO) directly enhanced the LAC of attapulgite-based composites. This mirrors our central finding that incorporating moderate-Z manganese (Z = 25) is the most effective strategy for boosting shielding performance, particularly at low energies.

Similarly, the approach in ref. 9 of doping a nano-bentonite matrix with the N–HgO filler to enhance attenuation is conceptually analogous to our strategy of substituting Mn into the AFO zeolite framework. Both studies confirm the universal principle that introducing elements with higher atomic numbers is a powerful lever for improving gamma-ray shielding.

The experimental and simulation results from these recent studies on composites[7–9] provide a broader context for our theoretical predictions. They validate the general methodology of enhancing a base material with specific additives, thereby strengthening confidence in the predicted performance of our strategically substituted zeolite frameworks. The strong agreement between the design principles and the resulting performance trends across these different material classes underscores the robustness and potential of our computational findings.

4. Conclusions

This study systematically investigated the gamma-ray shielding properties of AlPO-41 and its derivatives (SAPO-41, MnAPO-41, and MnAPSO-41), demonstrating that strategic elemental substitution is a powerful strategy for designing high-performance shielding materials. This work provides a significant conceptual and methodological advancement by establishing the AFO zeolite as a tunable platform for radiation shielding, moving beyond its traditional exploration for catalytic applications. We have quantitatively demonstrated how strategic elemental substitution directly controls shielding performance. The key findings are as follows:

- Among the studied compositions, MnAPO-41 emerged as the most effective shield, achieving the highest density (3.897 g cm^{-3}) and the highest effective atomic number (Z_{eff} = 14.96 at 15 keV), with a MAC of 9.064 $cm^2\ g^{-1}$ at 15 keV that is notably superior to the base AlPO-41 framework.
- The shielding performance is strongly energy-dependent. The high-Z contribution of Mn provides exceptional attenuation *via* the photoelectric effect at low energies ($E < 0.15$ MeV), while the increased density of Mn- and Si-substituted frameworks ensures continued superior performance in the intermediate energy regime (0.2–5.0 MeV) where Compton scattering dominates.
- A clear positive correlation between material density and shielding performance was established, with a performance threshold identified for frameworks with densities above $\sim$3.89 g cm^{-3}.
- This pinpoints a clear design strategy: maximizing density through Mn substitution is the primary route for optimal attenuation, while Si co-substitution offers valuable tunability for balancing structural and functional properties.

Thus, the Mn-substituted AFO zeolite frameworks, particularly MnAPO-41, successfully combine a lightweight porous architecture with high shielding efficiency. This unique combination makes them outstanding candidates for advanced radiation protection, with direct implications for several critical sectors:

- Spacecraft shielding: the low mass is paramount for reducing launch costs. These zeolites could be integrated as filler materials within composite wall panels or as a coating on internal structures to protect astronauts from galactic cosmic rays and solar particle events without adding excessive weight.
- Medical applications: in diagnostic imaging (*e.g.*, PET and SPECT) and radiation therapy rooms, these materials could be used to fabricate lightweight, lead-free mobile shields, protective barriers, or even components within imaging devices where weight and portability are concerns.
- Nuclear energy: for portable instrumentation, personal protective equipment (PPE) like aprons and gloves, and for lining specific compartments in nuclear facilities, these zeolites offer a non-toxic, manageable alternative to lead.

However, the path to practical deployment presents foreseeable challenges that must be addressed in future work. These include the following:

- Scale-up synthesis: the hydrothermal synthesis of phase-pure AFO frameworks at a large scale and cost-effective price needs to be optimized.
- Formulation and integration: the zeolite powders must be effectively integrated into a durable matrix (*e.g.*, polymers, ceramics, or metals) to form macroscopic shields without compromising their attenuation properties or mechanical integrity.
- Stability: the long-term thermal, radiation, and mechanical stability of these frameworks under operational conditions (*e.g.*, in a space vacuum or in a high-radiation environment) requires thorough experimental investigation.

This work establishes a foundational principle for the rational design of next-generation shielding materials and outlines a clear path forward, from atomic-scale simulation to addressing the practical challenges of real-world application.

Conflicts of interest

There are no conflicts to declare.

Data availability

The datasets generated and/or analyzed during the current study are available from the corresponding author upon reasonable request. All relevant computational input files, raw data, and processed results will be shared with editors or reviewers if required for verification purposes.

Supplementary information (SI) is available. See DOI: **https://doi.org/10.1039/d5ma01077b**.

Acknowledgements

Z. Y. Khattari would like to thank The Hashemite University for financial support. During the preparation of this work the author used ChatGPT/Open AI in order to improve the manuscript English language and grammar. After using this tool/service, the author reviewed and edited the content as needed and takes full responsibility for the content of the publication.

References

1 A. B. Chilton, J. K. Shultis and R. Faw, *Principles of Radiation Shielding*, 1st edn, Prentice-Hall, Englewood Cliffs, New Jersey, 1984.
2 J. R. Lamarsh and A. J. Baratta, *Introduction to Nuclear Engineering*, 4th edn, Pearson, 2017.
3 N. M. Azreen, R. S. M. Rashid, M. Haniza, Y. L. Voo and Y. H. M. Amran, *Constr. Build. Mater.*, 2018, **172**, 370–377.
4 S. M. R. Abdar Esfahani, *et al.*, *J. Build. Eng.*, 2021, **33**, 101615.
5 I. Sims, J. Lay and J. Ferrari, in *Lea's Chemistry of Cement and Concrete*, ed. P. C. Hewlett and M. Liska, *Butterworth-Heinemann*, 5th edn, 2019, pp. 699–778.
6 T. Kundu, L. Gilmanova, W. F. Yong and S. Kaskel, in *Porous Materials for Environmental Applications*, Springer, Cham, 2021, pp. 1–39.
7 R. M. El-Sharkawy, M. Almeshari, Y. Alzamil, A. Abanomy, B. Alshoumr, A. M. Halbas, E. A. Allam, M. E. Mahmoud, H. A. Saudi and A. El-Taher, *Mater. Adv.*, 2025, **6**, 4568–4581, DOI: **10.1039/D5MA00287G**.
8 M. Sayed, E. A. Allam, M. E. Mahmoud, R. M. El-Sharkawy, K. A. Mahmoud, S. M. Shaaban, R. A. Elsad and I. M. Nabil, *Radiat. Phys. Chem.*, 2025, **236**, 112917, DOI: **10.1016/j.radphyschem.2025.112917**.
9 A. El-Taher, H. M. H. Zakaly, E. A. Allam, R. M. El-Sharkawy, M. Al Meshari, A. M. Soliman, M. Salih, H. Alahmad and M. E. Mahmoud, *Radiat. Phys. Chem.*, 2025, **229**, 112409, DOI: **10.1016/j.radphyschem.2024.112409**.
10 R. M. Kirchner and J. M. Bennett, *Zeolites*, 1994, **14**, 523–528.
11 S. Caldarelli, A. Anton Meden and A. Tuel, *J. Phys. Chem. B*, 1999, **103**, 5477–5487.
12 M. Hartmann, A. M. Prakash and L. Kevan, *J. Chem. Soc., Faraday Trans.*, 1998, **94**, 723–727.
13 R. K. Guntu, *Ceram. Int.*, 2025, **51**(Part B), 16524–16538.
14 S. Al-Omari, F. Afaneh and Z. Y. Khattari, *Opt. Mater.*, 2024, **152**, 115548.
15 R. K. Elastic Guntu, *Bull. Mater. Sci.*, 2019, **42**, 214.
16 Z. Y. Khattari, *J. Am. Ceram. Soc.*, 2024, **107**, 3761–3768.
17 R. K. Guntu, *J. Mol. Liq.*, 2024, **401**, 124685.
18 S. Al-Omari, F. Afaneh, R. A. Elsad, Y. S. Rammah and Z. Y. Khattari, *Radiat. Phys. Chem.*, 2024, **215**, 111377.
19 Z. Y. Khattari, *J. Mater. Sci.: Mater. Electron.*, 2025, **36**, 845.
20 N. Şahin, *et al.*, *Prog. Nucl. Energy*, 2021, **135**, 103703.
21 Z. Y. Khattari, *Opt. Mater.*, 2024, **150**, 115197.
22 S. Al-Omari, F. Afaneh and Z. Y. Khattari, *J. Am. Ceram. Soc.*, 2024, **107**, 7224–7236.
23 Z. Y. Khattari, *Silicon*, 2024, **16**, 1753–1764.
24 S. Al-Omari, A. Alameri, F. Afaneh and Z. Y. Khattari, *Opt. Mater.*, 2024, **152**, 115477.
25 Z. Y. Khattari, *Silicon*, 2025, **17**, 2781–2796.
26 F. Afaneh, S. Al-Omari, G. ALMisned, H. O. Tekin and Z. Y. Khattari, *Radiat. Phys. Chem.*, 2025, **226**, 112232.
27 Z. Y. Khattari, *Silicon*, 2025, **17**, 1639–1656.
28 Z. Y. Khattari, *J. Am. Ceram. Soc.*, 2025, **108**, e20560.